Hindawi
Shock and Vibration
Volume 2018, Article ID 2497035, 11 pages
https://doi.org/10.1155/2018/2497035

Research Article

Dynamics of a Upright Pole Coupled with Nonlinear Hysteretic Isolators under Harmonic Base Excitation

Yongfeng Cheng,[1] Hulun Guo ,[2,3] Zhubing Zhu,[1] Xiaochao Su,[4] and Yushu Chen[2,3,4]

[1]*China Electric Power Research Institute, Beijing 100192, China*
[2]*Department of Mechanics, Tianjin University, Tianjin 300072, China*
[3]*Tianjin Key Laboratory of Nonlinear Dynamics and Control, Tianjin 300072, China*
[4]*School of Astronautics, Harbin Institute of Technology, Harbin 150001, China*

Correspondence should be addressed to Hulun Guo; hlguo@tju.edu.cn

Received 7 April 2018; Accepted 16 May 2018; Published 13 June 2018

Academic Editor: Gloria Terenzi

Leady isolator shows hysteretic nonlinearity. The isolation efficiency of leady isolator is an important problem in many engineering structures. In this paper, vibrations of a ceramic upright pole coupled with four leady isolators under harmonic base excitation are studied. A hysteretic force-deformation model of leady isolator is derived from experimental results. With this model, the vibration of the pole in rotation is studied. The frequency response is obtained analytically by employing harmonic balance method. The analytical results are agreed well with numerical results. The vibration of the pole is decreased greatly by leady isolator, especially near resonant case. The influences of system parameters on vibration response and resonant peak are discussed in detail.

1. Introduction

High voltage insulator is widely used in transmission equipment. They are usually designed as slender upright pole; see Figure 1. Such engineering structures often suffer various base excitation. The stability and vibration of these structures under base excitation are an important problem.

Dynamics of a structure subjected base excitation were studied by many authors. Shenton and Jones [1] present the general, two-dimensional formulation for the response of free-standing rigid bodies to base excitation. They gave a complete and consistent formulation for five possible modes of response (rest, slide, rock, slide-rock, and free flight) and impact between the body and foundation. Capecchi et al. [2] used numerical method to study the asymptotic response of a rigid block to harmonic force. Huang et al. [3] employing the incremental harmonic balance (IHB) method studied the nonlinear steady-state response of a curved beam subject to uniform base harmonic excitation with both quadratic and cubic nonlinearities. Kocatürk [4] analyzed the steady-state response with respect to base movement of a viscoelastically supported cantilever beam. Ervin and Wickert [5] investigated the forced complex responses of a clamped-clamped beam attached a rigid body, subjected to base excitation. Periodic responses, period-doubling bifurcations, grazing impacts, subharmonic regions, fractional harmonic resonances, and apparently chaotic responses were found in this system. Feng et al. [6] investigated the nonlinear motion of a slender cantilever beam subject to axial narrow-band random excitation.

Because of the complex dynamics of cantilever beam due to base excitation, vibration suppression of cantilever beam is of great practical interest in industrial sector. Sometimes, tip mass modify the vibrating behavior of cantilever beam. Esmailzadeh and Nakhaie-Jazar[7] studied the periodic behavior of a cantilever beam with end mass subjected to harmonic base excitation by using Green's function and employing Schauder's fixed point theorem. Sayag and Dowell [8] computationally and experimentally studied a cantilever beam with a tip mass under base excitation. Damping and yield stress of the beam were both considered. They observed that the damping was likely nonlinear. Eftekhari et al. [9] investigated the vibration suppression of a symmetrically cantilever composite beam coupled with an oscillator at the tip using internal resonance under chordwise base excitation.

Figure 1: High voltage insulator.

Figure 2: Leady isolator.

However, tip mass or oscillator attached on the top of high voltage insulator is hard to realize. An isolator attached on the bottom of high voltage insulator is more realizable. New structures were applied in many nonlinear isolators. Han et al. [10] presented a nonlinear isolator constituted by three linear spring. They found complex equilibrium bifurcations in this system. Xu et al. [11] designed a nonlinear magnetic low-frequency vibration isolator with the characteristic of quasi-zero stiffness. Zheng et al. [12] employed a negative stiffness magnetic spring to reduce the resonance frequency of linear isolator. Liu et al. [13] designed a negative stiffness corrector which is formed by Euler buckled beams and studied the characteristics of this passive nonlinear isolator. Huang et al. [14] analytically and experimentally studied the vibration isolation characteristics of a nonlinear isolator using Euler buckled beams as negative stiffness corrector. Friswell and Flores [15] investigated the design of nonlinear high-static-low-dynamic-stiffness isolation mounts using beams of tunable geometric nonlinear stiffness. Dutta and Chakraborty [16] studied the effectiveness of a nonlinear isolator with magneto rheological damper (MR). The MR damper was modeled including Bouc-Wen hysteretic element and the spring was modeled by cubic nonlinearity. Jangid and Datta [17] investigated the dissipation of hysteretic energy in the isolator of the base isolated structure under seismic excitation. Zhu et al. [18] used the quasistatic method and digital simulation studied the stationary response of smooth and bilinear hysteretic systems to narrow-band random excitations. Samani et al. [19] investigated the effect of dynamic loading on hysteretic behavior of a special kind of frictional damper (cylindrical frictional damper) by experimental and numerical methods.

New materials were also used to constitute nonlinear isolators. Heertjes and van de Wouw [20] studied the nonlinear dynamics of a single-degree-of-freedom pneumatic vibration isolator. Based on a physical model, the stiffness property of the isolator was described by a nonsymmetric stiffness nonlinearity. Chen et al. [21] used nonlinear polynomial functions to present the stiffness and damper of rubber isolators. The coefficients were identified by experimental data. Wang and Zheng [22] studied the coupling vibration of nonlinear isolators and two flexible beams by experimental and analytical methods. Shaska et al. [23] explored the advantages and characteristics of nonlinear butyl rubber isolators in vibratory shear by comparison with linear isolators. Nonlinear characteristics in shear deformation, which was dependent on frequency and temperature, were reflected on stiffness and damping. Carboni et al. [24] found that rheological device provided nonlinear hysteretic forces to a one-degree-of-freedom mass through suitable assemblies of NiTiNOL and steel wire ropes subject to tension-flexure cycles. Then, they studied the frequency-response curves of the isolator system subject to base excitation numerically and experimentally [25]. The dynamic responses of a multistory steel building model were also mitigated well [26]. Jiang and Yuan [27] studied the finite element matrix updating problem in a hysteretic damping model based on measured incomplete vibration modal data.

In order to study the vibration problem of a hysteretic system, averaging method was employed by Ding et al. [28]. They integrated the hysteretic function in period by using averaging method. Harmonic balance method can also solve hysteretic problems. Xiong et al. [29] used incremental harmonic balance method to analyze the vibration of a nonlinear system with the bilinear hysteretic oscillator. Based on these methods, we employ the harmonic balance method to investigate the dynamical behavior of a upright pole coupled with leady isolators (see Figure 2) under harmonic base excitation. Firstly, a hysteretic force-deformation model of leady isolator is derived from experimental results. With this model, the dynamic model of upright pole in rotation is established. Then, the frequency response is obtained analytically by employing harmonic balance method. The analytical results are compared with numerical results. Lastly, the influences of system parameters on vibration response and resonant peak are discussed in detail.

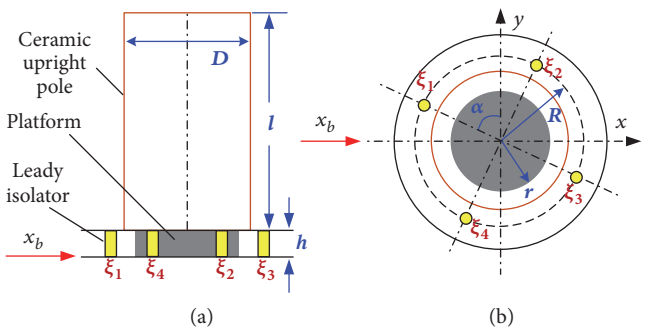

FIGURE 3: Geometry of ceramic upright pole: (a) side view; (b) top view.

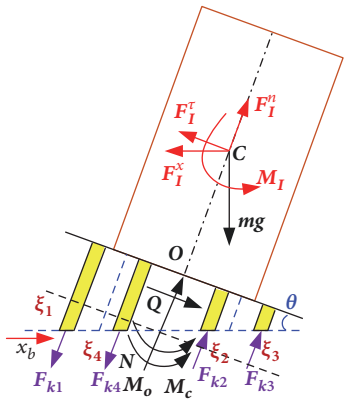

FIGURE 4: Dynamic equilibrium of ceramic upright pole under base excitation.

2. Dynamic Model

The model considered is shown in Figure 3. It consists of a ceramic upright pole located on an elastic circular platform, and four leady isolators are uniformly distributed around the platform. The upright pole is considered as a rigid body. Its density is ρ, and length is l. The Young's modulus, diameter, and thickness of the platform are E, r, and h, respectively. The space between leady isolators and central point is R. The base moves as x_b in x direction. The angle between the first isolator ξ_1 and y direction is α which will be $0 < \alpha < \pi/2$.

All forces of the upright pole under base excitation are shown in Figure 4. Due to base excitation, the upright pole will rotate around point O, and point O moves with the base as x_b. The rotating angle of the upright pole is θ. Deformation of four isolators are

$$\begin{aligned} \xi_1 &= \xi_3 = \theta R \sin\alpha \\ \xi_2 &= \xi_4 = \theta R \cos\alpha \end{aligned} \tag{1}$$

The forces from the platform can be simplified on point O as supporting force N, shear force Q, damping M_c, and moment M_O. The damping and moment can be obtained from

$$\begin{aligned} M_c &= c\dot{\theta} \\ M_O &= \int_{-r}^{r} E\frac{\theta y^2}{h} 2\sqrt{r^2 - x^2}\, dx = \frac{\pi E r^4}{4h}\theta \end{aligned} \tag{2}$$

There are four elastic forces F_{ki} when the isolators are stretched or constringent. We consider that there are no deformation of four isolators when the upright pole is static. In this case, the elastic forces of four isolators are zero, and the supporting force N from platform is equal to the gravity of the upright pole mg. When the base is moving, the inertia forces of the upright pole are $F_I^x = m\ddot{x}_b$, $F_I^n = (1/2)ml\dot{\theta}^2$, and $F_I^\tau = (1/2)ml\ddot{\theta}$, and the inertia moment is $M_I = (1/12)ml^2\ddot{\theta}$. Then, the governing equation of the upright pole in rotating can be written:

$$\begin{aligned} &\frac{1}{12}ml^2\ddot{\theta} - mg\frac{l}{2}\sin\theta + m\ddot{x}_b\frac{l}{2}\cos\theta + \frac{1}{2}ml\ddot{\theta}\frac{l}{2} + M_c \\ &\quad + M_O + F_{k1}R\sin\alpha + F_{k3}R\sin\alpha + F_{k2}R\cos\alpha \\ &\quad + F_{k4}R\cos\alpha = 0 \end{aligned} \tag{3}$$

According to experimental results, the elastic force of leady isolator appears hysteresis nonlinearity. The load-deformation curve is shown in Figure 5(a). The blue line is obtained from experiment, and the black line is approximately fitted curve. The slopes k_1 and k_2 are 2.3 kN/mm and 220 kN/mm, respectively. The max deformation ξ_m and middle break point deformation ξ_d are dependent on the max loading.

Figure 5(b) shows that the deformation varies with different loading. If the max loading is lower than F_0, the deformation varies between $(-\xi_0, \xi_0)$. The deformation and loading vary as the red route. In this case, the isolator shows as a linear spring, and the elastic coefficient is k_2. According to experimental results, ξ_0 is 0.206 mm, and F_0 is 22.70 kN. If the max loading is higher than F_0, the isolator shows hysteresis nonlinearity. The deformation of isolator changes with the loading in four linear segments which enclose an area. For example, if the max loading of the first and third isolators is F_{sm}, the displacement and loading vary as the black route, and if the max loading of the second and fourth isolators is F_{cm}, the displacement and loading vary as the blue route.

When the base excitation is harmonic, the rotating angle θ is periodic. Assuming the amplitude of θ being θ_m, the max ξ_1, ξ_3, are $\xi_{sm}=\theta_m R\sin\alpha$, and the max ξ_2, ξ_4, are $\xi_{cm}=\theta_m R\cos\alpha$.

If $\xi_{sm} < \xi_0$, the first and third isolators are linear.

$$F_{k1} = F_{k3} = k_2\theta R\sin\alpha \tag{4}$$

If $\xi_{sm} > \xi_0$, the first and third isolators are hysteresis.

$$F_{k1} = F_{k3} = \begin{cases} k_1(\theta R\sin\alpha + \xi_{sd}) + F_{sd} & -\xi_{sd} < \theta R\sin\alpha < \xi_{sm}, \theta\uparrow \\ k_2(\theta R\sin\alpha - \xi_{sm}) + F_{sm} & \xi_{sd} < \theta R\sin\alpha < \xi_{sm}, \theta\downarrow \\ k_1(\theta R\sin\alpha - \xi_{sd}) - F_{sd} & -\xi_{sm} < \theta R\sin\alpha < \xi_{sd}, \theta\downarrow \\ k_2(\theta R\sin\alpha + \xi_{sm}) - F_{sm} & -\xi_{sm} < \theta R\sin\alpha < -\xi_{sd}, \theta\uparrow \end{cases} \tag{5}$$

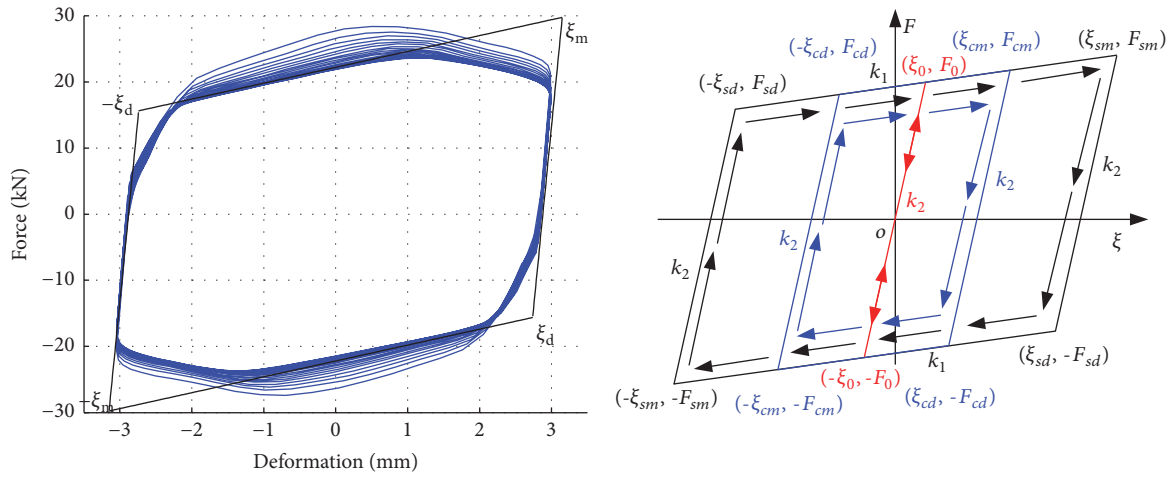

(a) Experimental results (b) Dynamic evolution

FIGURE 5: The load-deformation curve of leady isolator.

If $\xi_{cm} < \xi_0$, the second and fourth isolators are linear.

$$F_{k2} = F_{k4} = k_2 \theta R \cos\alpha \tag{6}$$

If $\xi_{cm} > \xi_0$, the second and fourth isolators are hysteresis.

$$F_{k2} = F_{k4} = \begin{cases} k_1(\theta R\sin\alpha + \xi_{cd}) + F_{cd} & -\xi_{cd} < \theta R\cos\alpha < \xi_{cm}, \theta \uparrow \\ k_2(\theta R\sin\alpha - \xi_{cm}) + F_{cm} & \xi_{cd} < \theta R\cos\alpha < \xi_{cm}, \theta \downarrow \\ k_1(\theta R\sin\alpha - \xi_{cd}) - F_{cd} & -\xi_{cm} < \theta R\cos\alpha < \xi_{cd}, \theta \downarrow \\ k_2(\theta R\sin\alpha + \xi_{cm}) - F_{cm} & -\xi_{cm} < \theta R\cos\alpha < -\xi_{cd}, \theta \uparrow \end{cases} \tag{7}$$

In order to simplify (5) and (7), the following equations can be obtained from Figure 5(b):

$$\begin{aligned} \xi_{sd} &= \xi_{sm} - 2\xi_0, \\ F_{sm} &= (k_2 - k_1)\xi_0 + k_1\xi_{sm}, \\ F_{sd} &= (k_2 + k_1)\xi_0 - k_1\xi_{sm} \\ \xi_{cd} &= \xi_{cm} - 2\xi_0, \\ F_{cm} &= 2(k_1 + k_2)\xi_0 - k_1\xi_{cm}, \\ F_{cd} &= (k_2 - k_1)\xi_0 + k_1\xi_{cm} \end{aligned} \tag{8}$$

Thus, the elastic forces from isolators can be expressed as

$$\begin{aligned} F_{k1} &= F_{k3} = G_s R\sin\alpha \\ F_{k2} &= F_{k4} = G_c R\cos\alpha \end{aligned} \tag{9}$$

where G_s and G_c are dependent on θ_m and isolator parameters.

$$G_s = \begin{cases} k_2\theta & \theta_m < \theta_{s0} \\ H_s(\theta) & \theta_m > \theta_{s0} \end{cases} \tag{10}$$

$$G_c = \begin{cases} k_2\theta & \theta_m < \theta_{c0} \\ H_c(\theta) & \theta_m > \theta_{c0} \end{cases} \tag{11}$$

where $\theta_{s0} = \xi_0/R\sin\alpha$, $\theta_{c0} = \xi_0/R\cos\alpha$, $\Delta k = k_2 - k_1$,

$$H_s(\theta) = \begin{cases} k_1\theta + \Delta k\theta_{s0} & -\theta_m + 2\theta_{s0} < \theta < \theta_m, \theta \uparrow \\ k_2\theta - \Delta k(\theta_m - \theta_{s0}) & \theta_m - 2\theta_{s0} < \theta < \theta_m, \theta \downarrow \\ k_1\theta - \Delta k\theta_{s0} & -\theta_m < \theta < \theta_m - 2\theta_{s0}, \theta \downarrow \\ k_2\theta + \Delta k(\theta_m - \theta_{s0}) & -\theta_m < \theta < -\theta_m + 2\theta_{s0}, \theta \uparrow \end{cases} \tag{12}$$

$$H_c(\theta) = \begin{cases} k_1\theta + \Delta k\theta_{c0} & -\theta_m + 2\theta_{c0} < \theta < \theta_m, \theta \uparrow \\ k_2\theta - \Delta k(\theta_m - \theta_{c0}) & \theta_m - 2\theta_{c0} < \theta < \theta_m, \theta \downarrow \\ k_1\theta - \Delta k\theta_{c0} & -\theta_m < \theta < \theta_m - 2\theta_{c0}, \theta \downarrow \\ k_2\theta + \Delta k(\theta_m - \theta_{c0}) & -\theta_m < \theta < -\theta_m + 2\theta_{c0}, \theta \uparrow \end{cases} \tag{13}$$

The small vibration of the upright pole is studied in this paper. We take the approximation: $\sin\theta \approx \theta$, $\cos\theta \approx 1$. Thus, the rotating equation of the upright pole with four leady isolators can be rewritten as

$$\begin{aligned} &\ddot{\theta} + 2c_0\omega_0\dot{\theta} + \omega_0^2\theta + \frac{6R^2}{ml^2}\left(G_s\sin^2\alpha + G_c\cos^2\alpha\right) \\ &\quad = -\frac{3}{2l}\ddot{x}_b \end{aligned} \tag{14}$$

where $\omega_0^2 = 3\pi Er^4/4hml^2 - 3g/2l$ and $c_0 = 3c/2\omega_0 ml^2$. If there is no isolator, $3\pi Er^4/4hml^2 - 3g/2l > 0$ is necessary for the stability of the upright pole.

3. Analytical Study

Since the base is excited by harmonic excitation, the acceleration of the base can be assumed

$$\ddot{x}_b = fg \sin \omega t \tag{15}$$

Then, a periodic response of θ is assumed to take the form

$$\theta = \theta_m \cos(\omega t + \varphi) \tag{16}$$

Substituting (16) into (10)-(13) and reserving the first order of Fourier expansion give

$$\begin{aligned} G_s &= a_1 \sin(\omega t + \varphi) + a_2 \cos(\omega t + \varphi) \\ G_c &= a_3 \sin(\omega t + \varphi) + a_4 \cos(\omega t + \varphi) \end{aligned} \tag{17}$$

where a_1, a_2, a_3, and a_4 can be obtained by integrating (10) and (11) over $\phi = \omega t + \varphi$ in one period.

$$\begin{aligned} a_1 &= \frac{1}{\pi}\int_{-\pi}^{\pi} G_s \sin\phi \, d\phi \\ &= \begin{cases} 0 & \theta_m < \theta_{s0} \\ \dfrac{1}{\pi}\displaystyle\int_{-\pi}^{\pi} H_s(\theta)\sin\phi \, d\phi & \theta_m > \theta_{s0} \end{cases} \end{aligned} \tag{18}$$

$$\begin{aligned} a_2 &= \frac{1}{\pi}\int_{-\pi}^{\pi} G_s \cos\phi \, d\phi \\ &= \begin{cases} k_2\theta_m & \theta_m < \theta_{s0} \\ \dfrac{1}{\pi}\displaystyle\int_{-\pi}^{\pi} H_s(\theta)\cos\phi \, d\phi & \theta_m > \theta_{s0} \end{cases} \end{aligned} \tag{19}$$

$$\begin{aligned} a_3 &= \frac{1}{\pi}\int_{-\pi}^{\pi} G_c \sin\phi \, d\phi \\ &= \begin{cases} 0 & \theta_m < \theta_{s0} \\ \dfrac{1}{\pi}\displaystyle\int_{-\pi}^{\pi} H_c(\theta)\sin\phi \, d\phi & \theta_m > \theta_{s0} \end{cases} \end{aligned} \tag{20}$$

$$\begin{aligned} a_4 &= \frac{1}{\pi}\int_{-\pi}^{\pi} G_c \cos\phi \, d\phi \\ &= \begin{cases} k_2\theta_m & \theta_m < \theta_{s0} \\ \dfrac{1}{\pi}\displaystyle\int_{-\pi}^{\pi} H_c(\theta)\cos\phi \, d\phi & \theta_m > \theta_{s0} \end{cases} \end{aligned} \tag{21}$$

When G_s and G_c are hysteresis, the variate θ in one period is shown in Figure 6. From Figure 5, we know that there are two break points during the deformation of each isolator varying in one period. The break point deformations of the first and third isolators are ξ_{sd} and -ξ_{sd}. The corresponding values of ϕ are ϕ_s and $-\pi+\phi_s$, where $\phi_s = \arccos(1-2\theta_{s0}/\theta_m)$. The variate θ in one period is divided into four segments. They represent four different stiffnesses of a hysteretic isolator

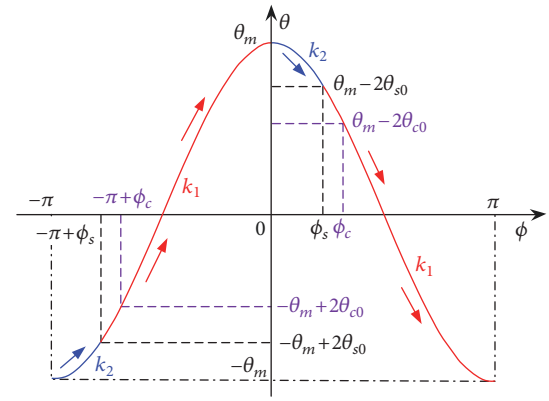

Figure 6: Vibration of θ in one period.

in four stages, respectively. Thus, the integrating of H_s can be obtained.

$$\begin{aligned} &\frac{1}{\pi}\int_{-\pi}^{\pi} H_s(\theta)\sin\phi \, d\phi \\ &= \frac{1}{\pi}\int_{-\pi}^{-\pi+\phi_s} \left(k_2\theta_m\cos\phi + \Delta k(\theta_m - \theta_{s0})\right)\sin\phi \, d\phi \\ &\quad + \frac{1}{\pi}\int_{-\pi+\phi_s}^{0} \left(k_1\theta_m\cos\phi + \Delta k\theta_{s0}\right)\sin\phi \, d\phi \\ &\quad + \frac{1}{\pi}\int_{0}^{\phi_s} \left(k_2\theta_m\cos\phi - \Delta k(\theta_m - \theta_{s0})\right)\sin\phi \, d\phi \\ &\quad + \frac{1}{\pi}\int_{\phi_s}^{\pi} \left(k_1\theta_m\cos\phi - \Delta k\theta_{s0}\right)\sin\phi \, d\phi \\ &= -\Delta k\theta_m\frac{1-\cos 2\phi_s}{2\pi} \end{aligned} \tag{22}$$

$$\begin{aligned} &\frac{1}{\pi}\int_{-\pi}^{\pi} H_s(\theta)\cos\phi \, d\phi \\ &= \frac{1}{\pi}\int_{-\pi}^{-\pi+\phi_s} \left(k_2\theta_m\cos\phi + \Delta k(\theta_m - \theta_{s0})\right)\cos\phi \, d\phi \\ &\quad + \frac{1}{\pi}\int_{-\pi+\phi_s}^{0} \left(k_1\theta_m\cos\phi + \Delta k\theta_{s0}\right)\cos\phi \, d\phi \\ &\quad + \frac{1}{\pi}\int_{0}^{\phi_s} \left(k_2\theta_m\cos\phi - \Delta k(\theta_m - \theta_{s0})\right)\cos\phi \, d\phi \\ &\quad + \frac{1}{\pi}\int_{\phi_s}^{\pi} \left(k_1\theta_m\cos\phi - \Delta k\theta_{s0}\right)\cos\phi \, d\phi \\ &= k_1\theta_m + \Delta k\theta_m\frac{2\phi_s - \sin 2\phi_s}{2\pi} \end{aligned} \tag{23}$$

The break point deformations of the second and fourth isolators are ξ_{cd} and -ξ_{cd}. The corresponding values of ϕ are

ϕ_c and $-\pi + \phi_c$, where $\phi_c = \arccos(1 - 2\theta_{c0}/\theta_m)$. Thus, the integrating of H_c can also be obtained.

$$\frac{1}{\pi}\int_{-\pi}^{\pi} H_c(\theta)\sin\phi\, d\phi = -\Delta k\theta_m \frac{1-\cos 2\phi_c}{2\pi} \quad (24)$$

$$\frac{1}{\pi}\int_{-\pi}^{\pi} H_c(\theta)\cos\phi\, d\phi = k_1\theta_m + \Delta k\theta_m \frac{2\phi_c - \sin 2\phi_c}{2\pi} \quad (25)$$

Substituting (15)-(17) into (14) and collecting the coefficients of $\cos\phi$ and $\sin\phi$ yield

$$\begin{aligned} &-\omega^2\theta_m + \omega_0^2\theta_m + \frac{6R^2}{ml^2}\left(a_2\sin^2\alpha + a_4\cos^2\alpha\right) \\ &\quad = \frac{3}{2l}fg\sin\varphi \\ &-2c_0\omega_0\omega\theta_m + \frac{6R^2}{ml^2}\left(a_1\sin^2\alpha + a_3\cos^2\alpha\right) \\ &\quad = -\frac{3}{2l}fg\cos\varphi \end{aligned} \quad (26)$$

Eliminating φ gives

$$\left(\omega^2\theta_m - \omega_0^2\theta_m - b_2b_4\right)^2 + \left(2c_0\omega_0\omega\theta_m - b_2b_3\right)^2 = b_1^2f^2 \quad (27)$$

where $b_1 = 3g/2l$, $b_2 = 6R^2/ml^2$, $b_3 = a_1\sin^2\alpha + a_3\cos^2\alpha$, and $b_4 = a_2\sin^2\alpha + a_4\cos^2\alpha$. Thus, the relationship between the amplitude of rotating angle θ and the excitation frequency of the base can be obtained analytically from (27).

4. Discussions on Dynamic Characteristics

In this section, analytical results and numerical results are compared, and dynamic characteristics are discussed. The influences of natural frequency of the pole and isolator parameters on dynamic response are also discussed. All the results of amplitude in rotating angle θ are presented in dB scale.

In this paper, the parameters without special statement are considered as $c_0 = 0.01$, $\omega_0 = 80$ Hz, $m = 980$ kg, $l = 2.8$ m, $\alpha = \pi/6$, R = 0.25 m, and $f = 0.5$, $g = 9.8$ m/s^2.

Analytical results and numerical results are compared in Figure 7. The dash line is the analytical result of the pole without isolator. It is a typical damped SDOF vibrator. The vibration amplitude becomes the max value as the excitation frequency ω near the natural frequency ω_0. The solid line and hollow dotted line are the analytical and numerical results of the pole with four isolators, respectively. They show that the analytical results are agreed well with the numerical results. More important, due to the leady isolator, the resonant frequency is increased, and resonant peak is decreased greatly.

In this case, $\alpha = \pi/6$, i.e., $\theta_{c0} < \theta_{s0}$. When $\theta_m < \theta_{c0}$, $G_s = G_c = k_2\theta$. The four isolators appear as linear spring. The natural frequency of this system is increased due to the linear stiffness of isolators. When $\theta_{c0} < \theta_m < \theta_{s0}$, $G_s = k_2\theta$, and G_c is hysteresis function. The natural frequency of this system is changed. The second and fourth isolators dissipate some of

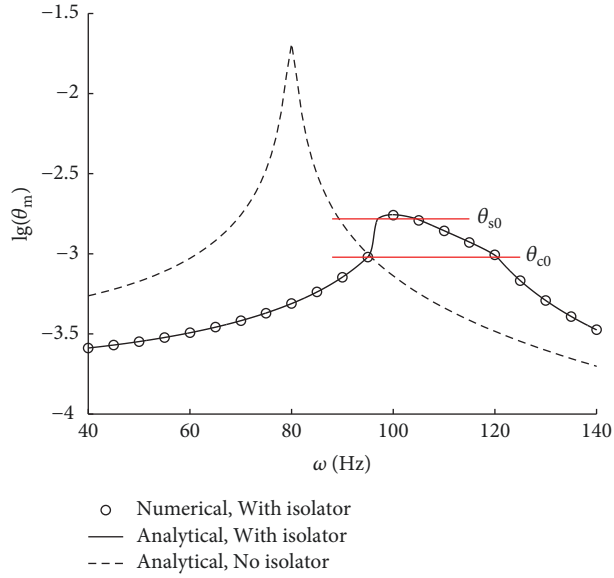

Figure 7: Influence of isolator on dynamic response.

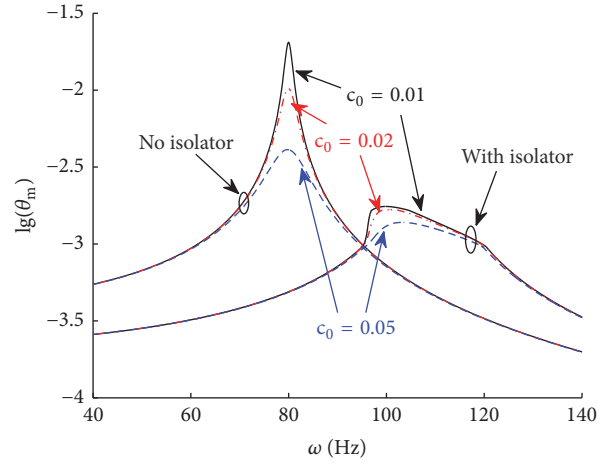

Figure 8: Effect of pole damping.

the vibration energy. The curve of amplitude versus frequency is inclined to lower frequency zone. When $\theta_m > \theta_{s0}$, both G_s and G_c are hysteresis. The vibration amplitude decreases greatly under resonant zone. This phenomenon is totally due to energy dissipation of the four isolators. The max amplitude of θ is determined by energy dissipation of isolators. It is an important parameter for vibration mitigation of upright pole when the base is excited by wide band frequency. The influence of different parameters on the max θ_m is studied in the following.

The effects of pole damping on the amplitude of θ are given in Figure 8. The cases both with isolator and without isolator are considered. The damping coefficient c_0 of pole is varied from 0.01 to 0.05. One can see that the vibration amplitude peak of the pole system either with or without isolator is decreased as pole damping increasing. More important, the max θ_m decreases 1.068 dB, 0.788 dB, and

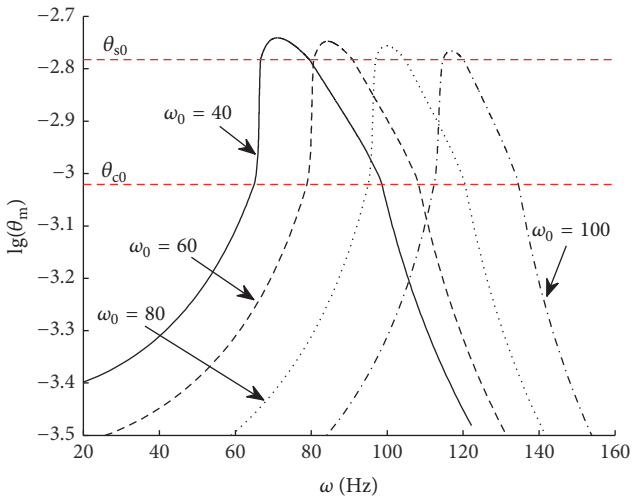

Figure 9: Effect of natural frequency.

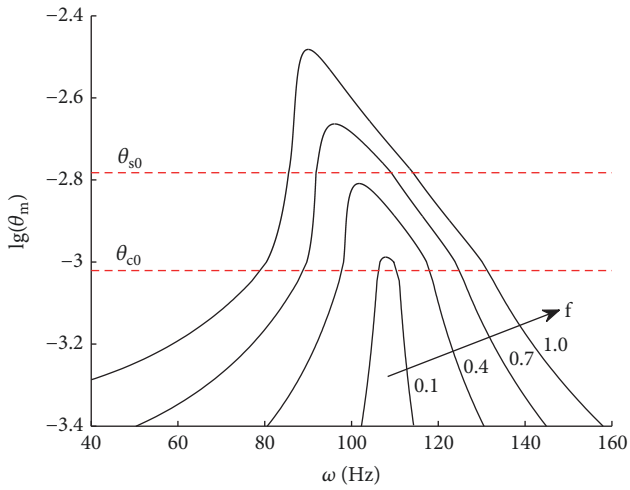

Figure 11: Effect of excitation amplitude.

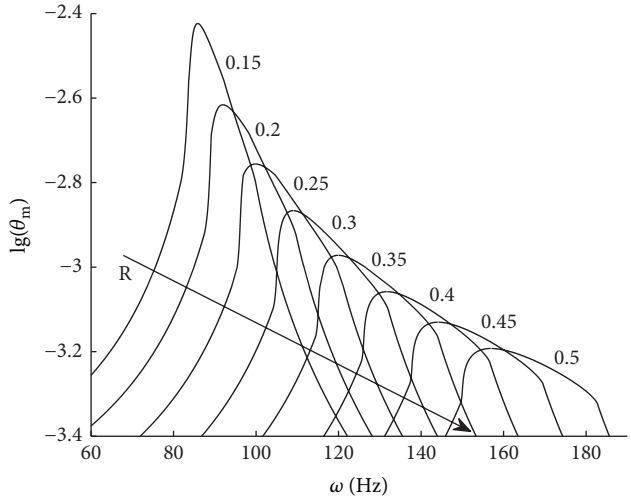

Figure 10: Effect of isolator space.

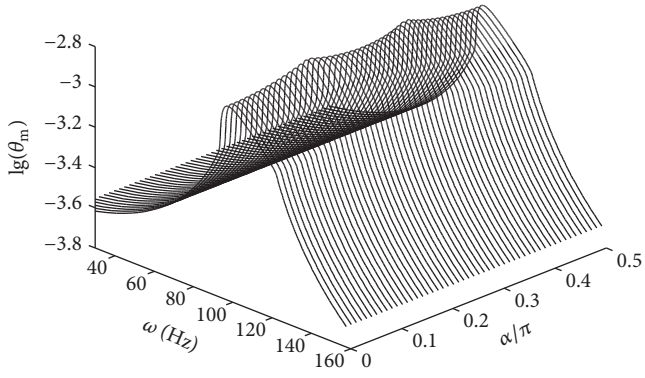

Figure 12: Effect of excitation direction.

0.473 dB due to isolator when the pole damping is 0.01, 0.02, and 0.05, respectively. It means that the smaller the pole damping the more decreasing of amplitude peak is caused by isolators.

Different amplitudes of θ are show in Figure 9 when the natural frequency is chosen as 40 Hz, 60 Hz, 80 Hz, and 100 Hz. The resonant frequency of the system increases as the natural frequency increased. Moreover, the max θ_m is slightly changed for different natural frequency.

Figure 10 shows θ_m vary with excitation frequency for different isolator space R. We can see that the resonant frequency is increased as the isolator space increased. More important, the vibration amplitude is decreased greatly when the isolator space is increased.

Given different excitation amplitude f, Figure 11 shows the amplitude of θ varies with excitation frequency. The vibration amplitude increases as the excitation amplitude increased. When the excitation amplitude is enough small, the max θ_m is larger than θ_{c0} but no more than θ_{s0}. It means that only the second and fourth isolators dissipate vibration energy, and the first and third isolators are vibrate in linear elasticity. Practically, the max θ_m is no more less θ_{c0}. The vibration amplitude will be infinite when the excitation frequency nears the resonant frequency without isolator. Due to energy dissipation of isolator, the vibration amplitude becomes a limit value. Only $\theta_m > \theta_{c0}$, and the isolator can dissipate vibration energy.

The amplitude-frequency curve for different excitation direction α is shown in three-dimensional space (see Figure 12). It can be seen that the resonant peak would be minimum when α is 0, $\pi/4$ or $\pi/2$. Which resonant peak is the smallest? It is an important problem for vibration mitigation, especially for the base excited by wide band frequency. Thus, the influence of different parameters on the max θ_m is studied in detail in the following.

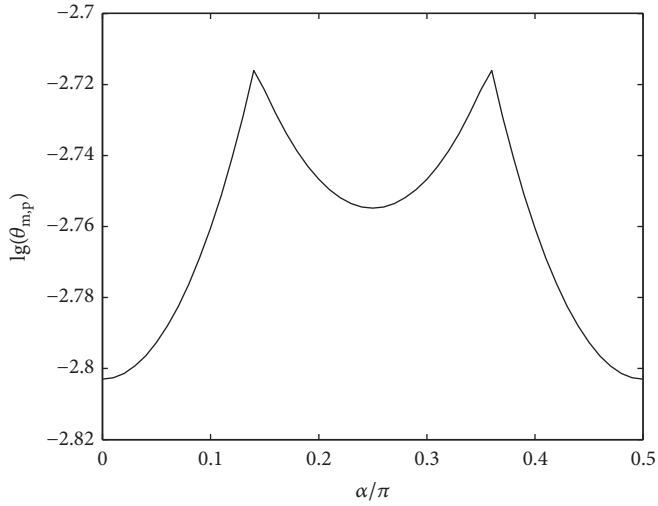

Figure 13: Influence of excitation direction on resonant peak.

5. Resonant Peak Analysis

In order to study the effect of isolator on resonant peak, the damping of the pole is omitted, i.e., $c_0 = 0$. Actually, when θ_m is the resonant peak, we have

$$\frac{d\theta_m}{d\omega} = 0 \tag{28}$$

Equations (27) and (28) imply

$$f^2 b_1^2 - b_2^2 b_3^2 = 0 \tag{29}$$

Thus, the resonant peak $\theta_{m,p}$ can be obtained.

$$\frac{fmgl}{4R^2} = \left| a_1 \sin^2\alpha + a_3 \cos^2\alpha \right| \tag{30}$$

In order to solve (30), we consider two cases: (1) $0 < \alpha < \pi/4$; (2) $\pi/4 < \alpha < \pi/2$.

Case (1) $0 < \alpha < \pi/4$, i.e., $\theta_{c0} < \theta_{s0}$.

If $\theta_{m,p} < \theta_{c0} < \theta_{s0}$, we have $a_1 = a_3 = 0$. There is no solution of resonant peak. Actually, according to the discussions in Section 4, we know that the resonant peak $\theta_{m,p}$ would be no more less the smaller one between θ_{s0} and θ_{c0}. Thus, this case will not happen.

If $\theta_{c0} < \theta_{m,p} < \theta_{s0}$, the resonant peak is

$$\theta_{m,p} = \frac{16\Delta k \xi_0^2}{16\Delta k \xi_0 R \cos\alpha - \pi fmgl} \tag{31}$$

Considering the amplitude of θ is positive, $16\Delta k \xi_0 R \cos\alpha - \pi fmgl > 0$ should be satisfied.

If $\theta_{c0} < \theta_{s0} < \theta_{m,p}$, the resonant peak is

$$\theta_{m,p} = \frac{32\Delta k \xi_0^2}{16\Delta k \xi_0 R (\sin\alpha + \cos\alpha) - \pi fmgl} \tag{32}$$

where $16\Delta k \xi_0 R(\sin\alpha + \cos\alpha) - \pi fmgl > 0$ should be satisfied.

Case (2) $\pi/4 < \alpha < \pi/2$, i.e., $\theta_{s0} < \theta_{c0}$.

If $\theta_{m,p} < \theta_{s0} < \theta_{c0}$, there is no solution of resonant peak.

If $\theta_{s0} < \theta_{m,p} < \theta_{c0}$, the resonant peak is

$$\theta_{m,p} = \frac{16\Delta k \xi_0^2}{16\Delta k \xi_0 R \sin\alpha - \pi fmgl} \tag{33}$$

where $16\Delta k \xi_0 R \sin\alpha - \pi fmgl > 0$ should be satisfied.

If $\theta_{s0} < \theta_{c0} < \theta_{m,p}$, the resonant peak is

$$\theta_{m,p} = \frac{32\Delta k \xi_0^2}{16\Delta k \xi_0 R (\sin\alpha + \cos\alpha) - \pi fmgl} \tag{34}$$

where $16\Delta k \xi_0 R(\sin\alpha + \cos\alpha) - \pi fmgl > 0$ should be satisfied.

Figure 13 shows the influence of excitation direction on resonant peak. We can conclude that when α is 0 or $\pi/2$, the resonant peak is the smallest. It means that two isolators have the largest deformation, and the most vibration energy is dissipated. But the other two isolators have no deformation.

Figures 14–17 show the influences of R, Δk, ξ_0, and f on the resonant peak. It can be seen that when $R < 0.087$ m, $\Delta k < 37.469$ kN/mm, $\xi_0 < 0.072$ mm, or $f > 1.436$, the resonant peak will be infinite. Otherwise, the resonant peak will be decreased as increasing R or Δk or decreasing f. It should be noticed that the resonant peak will decrease greatly and then increase rarely when ξ_0 increases from 0.072 mm. More important, the resonant peak will decrease greatly during special parameter intervals. We could conclude that the resonant peak is sensitive to these parameters within these parameter intervals. Outside these parameter intervals, the resonant peak is changed rarely as the parameter changing. Furthermore, we assume that $|d\theta_{m,p}/dp| > 0.01$ (p is one of the parameters R, Δk, ξ_0, or f), when the parameter is within the sensitive parameter interval. According to (31)-(34), we can obtain four sensitive parameter intervals: 0.087 m $< R <$ 0.292 m, 37.469 kN/mm $< \Delta k <$ 61.475 kN/mm, 0.072 mm

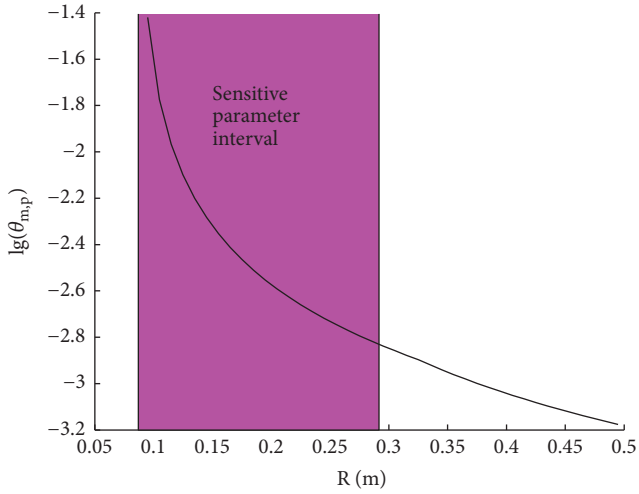

Figure 14: Influence of R on resonant peak.

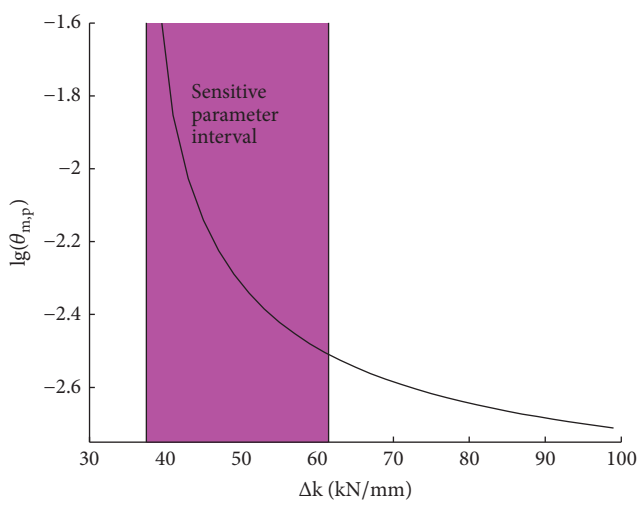

Figure 15: Influence of Δk on resonant peak.

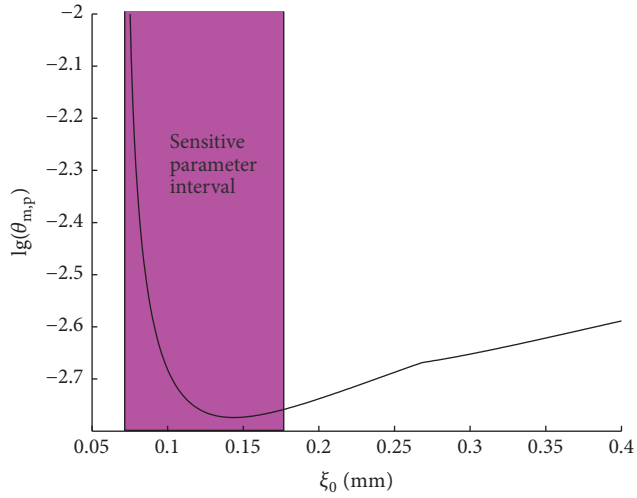

Figure 16: Influence of ξ_0 on resonant peak.

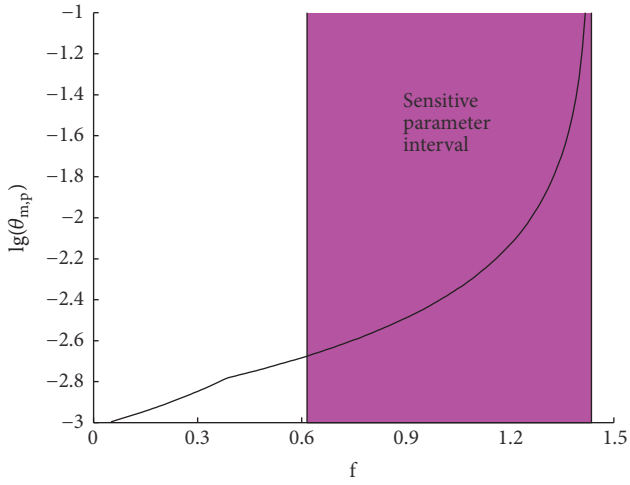

Figure 17: Influence of f on resonant peak.

$< \xi_0 <$ 0.177 mm, and $0.616 < f < 1.436$. The best parameters should be chosen outsider these sensitive parameter intervals.

From (31)-(34), we also found that the mass m and length l of the pole have the same effect as the excitation amplitude f. It means that decreasing m or l could also decrease the resonant peak of the pole. One should note that the gravity centre is in the middle of the pole where is $l/2$. Thus, decreasing the gravity centre also decreases the resonant peak. Figures 18 and 19 reveal the effects of the mass m and length l on the resonant peak. The sensitive parameter intervals of m and l are 1771 kg $< m <$ 2814 kg and 4.40 m $< l <$ 8.04 m, respectively.

6. Conclusions

The dynamical behavior of an upright pole coupled with four leady isolators under harmonic base excitation is addressed. Experimental results show that elastic force of leady isolator is hysteresis with deformation. Analytical solution of periodic response of the upright pole in rotating is obtained by employing harmonic balance method. The result is agreed well with numerical result. Both the analytical and numerical results show that the hysteresis in stiffness could dissipate vibration energy. The amplitude of the pole in rotating is decreased greatly, especially in resonant case. The smaller the pole damping is the more decreasing of amplitude peak is caused by isolators. Moreover, the natural frequency of the pole is almost independent of the resonant peak. In order to decrease the resonant peak of the pole, increasing the isolator space R or stiffness D-value of isolator Δk or decreasing the pole mass m, length l or excitation amplitude f would be viable. When isolators are installed in the excitation direction, energy dissipation would be maximum. More important, there are sensitive parameter intervals for all these parameters. Within the parameter interval, the resonant peak of upright pole could be decreased greatly. Outside the parameter interval, the resonant peak would be not sensitive to the parameter. The best parameters should be chosen outsider these sensitive parameter intervals.

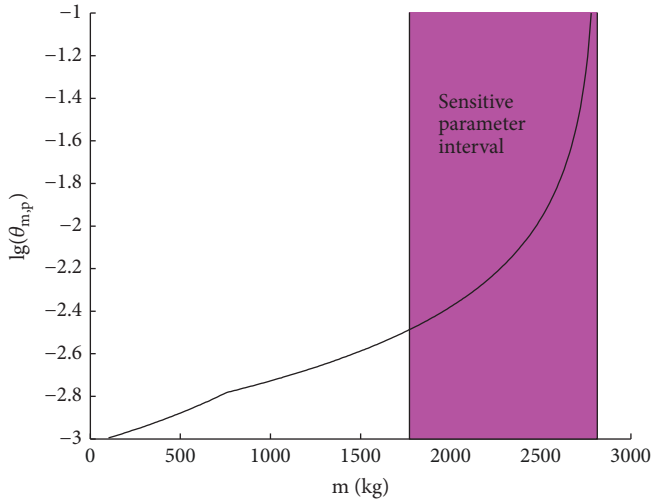

Figure 18: Influence of m on resonant peak.

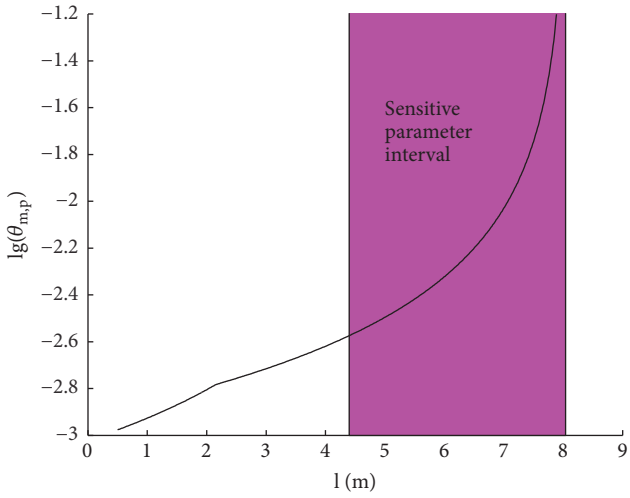

Figure 19: Influence of l on resonant peak.

Data Availability

The data used to support the findings of this study are available from the corresponding author upon request.

Conflicts of Interest

The authors declare that there are no conflicts of interest regarding the publication of this paper.

Acknowledgments

This study is funded by the National Natural Science Foundation of China (Grant no. 11302145), Tianjin Research Program of Application Foundation and Advanced Technology (Grant no. 15JCQNJC04900), and Scientific Research Program of SGCC: Research on Seismic Performance of Porcelain Pillar Electrical Equipment Based on Nonlinear Theory (Grant no. GCB17201700322).

References

[1] H. W. Shenton and N. P. Jones, "Base excitation of rigid bodies. I: formulation," *Journal of Engineering Mechanics*, vol. 117, no. 10, pp. 2286–2306, 1991.

[2] D. Capecchi, R. Giannini, and R. Masiani, "Motion of a rigid body with a rounded base due to harmonic excitation," *International Journal of Non-Linear Mechanics*, vol. 31, no. 2, pp. 175–191, 1996.

[3] J. L. Huang, R. K. L. Su, Y. Y. Lee, and S. H. Chen, "Nonlinear vibration of a curved beam under uniform base harmonic excitation with quadratic and cubic nonlinearities," *Journal of Sound and Vibration*, vol. 330, no. 21, pp. 5151–5164, 2011.

[4] T. Kocatürk, "Determination of the steady-state response of viscoelastically supported cantilever beam under sinusoidal base excitation," *Journal of Sound and Vibration*, vol. 281, no. 3-5, pp. 1145–1156, 2005.

[5] E. K. Ervin and J. A. Wickert, "Repetitive impact response of a beam structure subjected to harmonic base excitation," *Journal of Sound and Vibration*, vol. 307, no. 1-2, pp. 2–19, 2007.

[6] Z. H. Feng, X. J. Lan, and X. D. Zhu, "Principal parametric resonances of a slender cantilever beam subject to axial narrow-band random excitation of its base," *International Journal of Non-Linear Mechanics*, vol. 42, no. 10, pp. 1170–1185, 2007 (Chinese).

[7] E. Esmailzadeh and G. Nakhaie-Jazar, "Periodic behavior of a cantilever beam with end mass subjected to harmonic base excitation," *International Journal of Non-Linear Mechanics*, vol. 33, no. 4, pp. 567–577, 1998.

[8] M. R. Sayag and E. H. Dowell, "Linear Versus Nonlinear Response of a Cantilevered Beam under Harmonic Base Excitation: Theory and Experiment," *Journal of Applied Mechanics*, vol. 83, no. 10, 2016.

[9] M. Eftekhari, S. Ziaei-Rad, and M. Mahzoon, "Vibration suppression of a symmetrically cantilever composite beam using internal resonance under chordwise base excitation," *International Journal of Non-Linear Mechanics*, vol. 48, pp. 86–100, 2013.

[10] Y. Han, Q. Cao, and J. Ji, "Nonlinear dynamics of a smooth and discontinuous oscillator with multiple stability," *International*

Journal of Bifurcation and Chaos, vol. 25, no. 13, 1530038, 16 pages, 2015.

[11] D. L. Xu, Q. P. Yu, J. X. Zhou, and S. R. Bishop, "Theoretical and experimental analyses of a nonlinear magnetic vibration isolator with quasi-zero-stiffness characteristic," *Journal of Sound and Vibration*, vol. 332, no. 14, pp. 3377–3389, 2013.

[12] Y. Zheng, X. Zhang, Y. Luo, B. Yan, and C. Ma, "Design and experiment of a high-static-low-dynamic stiffness isolator using a negative stiffness magnetic spring," *Journal of Sound and Vibration*, vol. 360, pp. 31–52, 2016.

[13] X. T. Liu, X. C. Huang, and H. X. Hua, "On the characteristics of a quasi-zero stiffness isolator using Euler buckled beam as negative stiffness corrector," *Journal of Sound and Vibration*, vol. 332, no. 14, pp. 3359–3376, 2013.

[14] X. Huang, X. Liu, J. Sun, Z. Zhang, and H. Hua, "Vibration isolation characteristics of a nonlinear isolator using euler buckled beam as negative stiffness corrector: a theoretical and experimental study," *Journal of Sound and Vibration*, vol. 333, no. 4, pp. 1132–1148, 2014.

[15] M. I. Friswell and E. I. Saavedra Flores, "Dynamic isolation systems using tunable nonlinear stiffness beams," *The European Physical Journal Special Topics*, vol. 222, no. 7, pp. 1563–1573, 2013.

[16] S. Dutta and G. Chakraborty, "Performance analysis of nonlinear vibration isolator with magneto-rheological damper," *Journal of Sound and Vibration*, vol. 333, no. 20, pp. 5097–5114, 2014.

[17] R. S. Jangid and T. K. Datta, "Dissipation of Hysteretic Energy in Base Isolated Structure," *Shock and Vibration*, vol. 3, no. 5, pp. 353–359, 1996.

[18] W. Q. Zhu, C. D. Huang, and T. T. Soong, "Narrow-band excitation of hysteretic systems," *Shock and Vibration*, vol. 4, no. 4, pp. 241–250, 1997.

[19] H. Rahmani Samani, M. Mirtaheri, A. P. Zandi, and H. Bahai, "The effects of dynamic loading on hysteretic behavior of frictional dampers," *Shock and Vibration*, vol. 2014, 2014.

[20] M. Heertjes and N. van de Wouw, "Nonlinear dynamics and control of a pneumatic vibration isolator," *Journal of Vibration and Acoustics*, vol. 128, no. 4, pp. 439–448, 2006.

[21] C. Xueqian, S. Zhanpeng, H. Qinshu, D. Qiang, and L. Xin'en, "Influence of uncertainty and excitation amplitude on the vibration characteristics of rubber isolators," *Journal of Sound and Vibration*, vol. 377, pp. 216–225, 2016.

[22] G. Y. Wang and G. T. Zheng, "Vibration of two beams connected by nonlinear isolators: Analytical and experimental study," *Nonlinear Dynamics*, vol. 62, no. 3, pp. 507–519, 2010.

[23] K. Shaska, R. A. Ibrahim, and R. F. Gibson, "Influence of excitation amplitude on the characteristics of nonlinear butyl rubber isolators," *Nonlinear Dynamics*, vol. 47, no. 1-3, pp. 83–104, 2007.

[24] B. Carboni, W. Lacarbonara, and F. Auricchio, "Hysteresis of multiconfiguration assemblies of nitinol and steel strands: Experiments and phenomenological identification," *Journal of Engineering Mechanics*, vol. 141, no. 3, 2015.

[25] B. Carboni and W. Lacarbonara, "Nonlinear dynamic characterization of a new hysteretic device: experiments and computations," *Nonlinear Dynamics*, vol. 83, no. 1-2, pp. 23–39, 2016.

[26] B. Carboni and W. Lacarbonara, "Nonlinear vibration absorber with pinched hysteresis: Theory and experiments," *Journal of Engineering Mechanics*, vol. 142, no. 5, 2016.

[27] J. Jiang and Y. Yuan, "Updating Stiffness and Hysteretic Damping Matrices Using Measured Modal Data," *Shock and Vibration*, vol. 2018, pp. 1–7, 2018.

[28] Q. Ding, A. Y. T. Leung, and J. E. Cooper, "Dynamic analysis of a self-excited hysteretic system," *Journal of Sound and Vibration*, vol. 245, no. 1, pp. 151–164, 2001.

[29] H. Xiong, X. Kong, H. Li, and Z. Yang, "Vibration analysis of nonlinear systems with the bilinear hysteretic oscillator by using incremental harmonic balance method," *Communications in Nonlinear Science and Numerical Simulation*, vol. 42, pp. 437–450, 2017.